Structure and magnetic properties of hausmannite α-Mn_3O_4, metastable high-pressure marokite γ-Mn_3O_4, and defected α-Mn_3O_4

Björn Schwarz,* Julian Hansen, Anna-Lena Hansen, Eugen Zemlyanushin, and Helmut Ehrenberg
Institute for Applied Materials (IAM), Karlsruhe Institute of Technology (KIT), 76344 Eggenstein-Leopoldshafen, Germany

(Received 6 February 2023; revised 15 March 2023; accepted 22 June 2023; published 13 July 2023)

The magnetic properties of tetragonal α-Mn_3O_4 spinel, its metastable high-pressure modification γ-Mn_3O_4, and of an α-Mn_3O_4 modification with a high amount of lattice defects were investigated by direct current (dc) and alternating current (ac) magnetometry as well as by heat capacity measurements. An α-Mn_3O_4 phase modification with a high amount of lattice defects instead of the desired metastable high pressure γ-Mn_3O_4 phase might unintentionally be obtained after the high-pressure application. The obtained results clarify strongly contradictory reports about the dc susceptibility data of γ-Mn_3O_4 in the literature. Further, *in situ* low-temperature x-ray diffraction experiments from 150 to 275 K and Mn K-edge x-ray absorption spectroscopy experiments at 80 and 300 K do not indicate any structural transition to be coupled with the magnetic transition at 210 K for the given γ-Mn_3O_4 sample. This is in contradiction with what was concluded from powder neutron diffraction alone in the literature, where a coupled structural transition accompanied with large atomic displacements of a Mn species was claimed to be accompanied to the magnetic transition.

DOI: 10.1103/PhysRevB.108.014417

I. INTRODUCTION

Synthetic manganese oxides are of interest for many applications and are used as catalysts, cathode materials and supercapacitors in batteries, multiferroics, semiconductors, and many others (interested readers are referred to Ref. [1] and references therein). In particular, Mn_3O_4 and its derivatives have been the object of fundamental research regarding the magnetic properties due to its mixed-valence state consisting of Mn^{2+} and Mn^{3+}. Upon cooling, the cubic high-temperature spinel β-Mn_3O_4 (space group no. 225: $Fm\bar{3}m$) [2] transforms to α-Mn_3O_4 (hausmannite) that has a tetragonally deformed spinel structure (space group no. 141: $I4_1/amd$) [3–5] at about 1435 K. The magnetic structure of hausmannite was described by Kasper [6] and Boucher *et al.* [7] using neutron diffraction methods on polycrystalline material. Boucher *et al.* found a ferrimagnetic behavior with dominant antiferromagnetic coupling and an ordered net magnetic moment by susceptibility measurements. The Curie temperature, where ferrimagnetic ordering sets in, is reported as $T_C = 42.5$ K. Above 400 K, the inverse susceptibility exhibits a linear temperature progression. A Curie-Weiss fit returns a Weiss constant of -564 K and a paramagnetic moment of $\mu_{\text{eff}} = 5.27\ \mu_B$. The paramagnetic moment fits very well with the (average) spin-only paramagnetic moment $\mu_{\text{eff}}^{\text{calc}} = 5.24\ \mu_B$ per Mn ion calculated for two Mn^{3+} and one Mn^{2+}. From the ferrimagnetic low-temperature structure, it was deduced that the Mn^{3+} ions occupy the Jahn-Teller distorted octahedral sites and the Mn^{2+} ions occupy the tetrahedral sites, i.e., it is a "normal" spinel that can be written as $Mn^{2+}[Mn^{3+}Mn^{3+}]O_4$. A more detailed investigation of the magnetic structure by neutron diffraction on Mn_3O_4 single crystals has been done by Jensen and Nielsen [8]. Below the Curie temperature of $T_C = 41$ K, they found a magnetic unit cell that coincides with the chemical unit cell and another magnetic transition at 33 K to a magnetic structure that may be described in terms of an orthorhombic magnetic unit cell which consists of the chemical tetragonal unit cell, doubled in the [010] direction. By means of neutron diffraction, Chardon and Vigneron [9] further revealed that the low-temperature commensurate ferrimagnetic structure of α-Mn_3O_4 undergoes a commensurate-incommensurate magnetic transition at 33 K with a sinusoidal incommensurate part of the magnetic structure. Recently, Kemei *et al.* [10] revealed that further structural distortions occur upon magnetic ordering at 42 K by employing high-resolution variable-temperature synchrotron x-ray diffraction. They showed that tetragonal $I4_1/amd$ (α-Mn_3O_4) and orthorhombic $Fddd$ phases coexist with nearly equal fractions below the Curie temperature. Magnetodielectric and magnetoelastic properties [11] and magnetic excitations and orbital physics in the ferrimagnetic Mn_3O_4 spinels, for instance, have been investigated by Chung *et al.* [12].

At high pressure of about 11.5 GPa (stabilized up to ~48 GPa), Mn_3O_4 transforms into orthorhombic γ-Mn_3O_4 (space group no. 57: $Pbcm$) that is isostructural to the $CaMn_2^{3+}O_4$ mineral named "marokite" [13–20]. Darul *et al.* [21] report that they found the Mn_3O_4 spinel to transform to the marokite high-pressure modification at much milder conditions of only 7.2 GPa and 400 °C. By quenching, γ-Mn_3O_4 can be conserved in a metastable state at ambient pressure and at room temperature [15]. In this metastable phase, $Mn^{3+}O_6$ octahedra (two short, two medium, and two long Mn^{3+}-O bond distances) form one-dimensional edge-sharing chains along the *a* axis and zigzag chains along the *b* axis. Mn^{2+} ions are located within the cavities that are formed by the zigzag chains of the $Mn^{3+}O_6$ octahedra as $Mn^{2+}O_8$ units.

*Corresponding author: bjoern.schwarz@kit.edu

In addition to Raman spectroscopy [20], the metastable γ-Mn_3O_4 phase has been investigated regarding its magnetic structure and properties by Hirai *et al.* [22], applying neutron scattering, heat capacity, and magnetometry, and by Ovsyannikov *et al.* [1] concerning magnetic and other physical properties. Hirai *et al.* report a coupled magnetic and structural first-order phase transition at $T_N' = 210$ K with an *a*-axis doubled antiferromagnetic unit cell. The coupled structural phase transition is claimed to be accompanied by a lattice volume drop of 0.5(1)% and "giant atomic displacements" of the Mn^{2+} ions by 0.25 Å and of one crystallographic oxygen species O(3) by 0.16 Å. Heat capacity C_p measurements reveal a broad feature near 210 K, supporting the existence of a phase transition. The ordering T_N' was interpreted to only affect the Mn^{3+} ions, but not the Mn^{2+} moments that were supposed to remain paramagnetic down to approximately 55 K. At $T_N = 55$ K, a feature in the heat capacity signal is reported that points to an additional phase transition. According to corresponding broad Bragg reflections in the neutron diffraction pattern that are found below the transition, it is interpreted as the formation of an incommensurate finite Q (correlation length) magnetic structure of the Mn^{2+} moments. The susceptibility measurements for γ-Mn_3O_4 as obtained by Hirai *et al.* are not in agreement with their results from neutron scattering and heat capacity and they are in strong contrast to those found by Ovsyannikov *et al.*

Hirai *et al.* found a monotonically increasing susceptibility with decreasing temperature (Curie-Weiss behavior) without any change of progression with temperature when transiting from the paramagnetic to the "partial" antiferromagnetic phase (only Mn^{3+} moments contribute) around $T_N' = 210$ K (see Fig. 5 in Ref. [22]). This transition to a partial antiferromagnetically ordered state was revealed from powder neutron diffraction (PND) and heat capacity measurements and is supposed to also affect the susceptibility curve in some way, which was, however, not observed experimentally. At temperatures below approximately 44 K, the susceptibility is reported to rise rapidly and to exhibit a clear hysteresis between field-cooled (FC) and zero-field-cooled (ZFC) measurements, which is explained by ferromagnetism of the main phase. This finding is also in contradiction to their results from PND and heat capacity that both indicated the magnetic phase transition (that now also includes the Mn^{2+} moments) to occur at about 55 K, and not 44 K. The magnetic moment vs field scan at 20 K has a zero-field extrapolated remanent magnetic moment of about 1 μ_B per formula unit (f.u.). By profile analysis of reflections from neutron diffraction experiments, this ferromagnetic phase is assumed to have formed incommensurate short-range magnetic order regarding the Mn^{2+} moments.

In contrast to that, Ovsyannikov *et al.* report to have found two antiferromagnetic transitions at $T_N' \sim 200$ K and $T_N \sim 55$ K, indicated by a broad bend and a sharper peak in the magnetic susceptibility data, respectively, for γ-Mn_3O_4 (see Fig. 3 in Ref. [1]). These features were observed for magnetic fields ranging from 5 to 50 kOe. A magnetization vs magnetic field curve at 1.8 K up 2 kOe showed a nearly linear behavior (as typical for the paramagnetic state or antiferromagnetic ordering) with a very tiny hysteresis that is ascribed to a minor amount of ferromagnetic impurities present in the sample. From a Curie-Weiss fit above 300 K, a paramagnetic effective moment of 5.80 μ_B per Mn ion and a Weiss constant of −650 K (antiferromagnetic coupling) were determined. The fact that a ferromagnetic behavior was not found for γ-Mn_3O_4 at low temperature, in contradiction to what was reported by Ref. [22], is supposed to be caused by slightly different chemical compositions of the investigated γ-Mn_3O_4 compounds according to Ovsyannikov *et al.* [1]. Clarification of these inconsistent reports about the magnetic properties of γ-Mn_3O_4 in the literature will be one accomplishment of this work.

Recently, Kozlenko *et al.* [23] report an *in situ* high-pressure crystal and magnetic structure investigation of Mn_3O_4 by x-ray (37 GPa) and powder neutron diffraction (PND) (20 GPa). According to their results, tetragonal α-Mn_3O_4 transforms to γ-Mn_3O_4 via an intermediate orthorhombic $CaTi_2O_4$-type phase (space group no. 63: *Bbmm* symmetry). Besides a comprehensive study of the influence of pressure on the details of the magnetic structures in α-Mn_3O_4, the γ-Mn_3O_4 (*Pbcm*) phase has also been investigated at 20 GPa by PND. It has been found that the orthorhombic *Pbcm* crystal structure remained unchanged upon cooling down to 7 K without any further statements about crystallographic details. Most relevant for this work is the observed formation of an antiferromagnetic order of the Mn^{3+} spins that forms with a propagation vector $k = (1/2, 0, 0)$ below T_N=275 K, i.e., 30% higher with respect to $T_N' = 210$ K reported for the metastable orthorhombic *Pbcm* γ-Mn_3O_4 phase at ambient pressure [22]. Furthermore, below 50 K, the emergence of a new broad magnetic peak located at $d_{hkl} = 3.89$ Å was detected that is associated with the presence of the short-range magnetic order of Mn^{2+} ions, in agreement with others [22].

In this work, the magnetic properties of α-Mn_3O_4, γ-Mn_3O_4, and of an α-Mn_3O_4 modification that contains a high number of lattice defects were investigated by dc and ac magnetometry as well as by heat capacity. The systematic study of this series allows one to clarify the reason for inconsistent reports about the magnetic properties of γ-Mn_3O_4 in the literature. Furthermore, *in situ* low-temperature x-ray diffraction (XRD) measurements from 150 to 275 K and Mn K-edge synchrotron x-ray absorption spectroscopy (XAS) experiments at 80 and 300 K were performed to test whether a structural phase transition is coupled to the magnetic transition at about $T_N' = 210$ K in γ-Mn_3O_4. Such a coupled structural phase transition that was supposed to be accompanied by giant atomic displacements of Mn^{2+} and an O species was reported based on results from PND [22]. The predominant sensitivity for atomic structural changes of the here applied XRD and XAS methods represent an advantage over PND when it comes to the question whether a structural phase transition is coupled to a magnetic one. Especially in the case that the PND data set is of poor quality, the strong magnetic reflections emerging at the magnetic phase transition might falsely cause, as an artifact, small changes in the atomic structural model and the lattice parameters when whole pattern fitting routines (Rietveld) are used for evaluation. A PND data set of limited quality is easily obtained for metastable high pressure phases, as the here investigated γ-Mn_3O_4, that are only available in comparably small quantities in general.

II. EXPERIMENTAL METHODS

A. Synthesis

A polycrystalline powder sample named "spinel" consisting of phase pure α-Mn_3O_4 phase as verified by XRD analysis (see below) was synthesized via a hydrothermal route. An amount of 4.37 mmol potassium permanganate ($KMnO_4$, Sigma-Aldrich, purity $\geqslant$97%) was dissolved in 50 ml deionized water. 5.00 mmol of polyethylene glycol [$H(OCH_2CH_2)_nOH$ with average molar mass $\approx$400 g/mol, Sigma-Aldrich] was added slowly into the violet solution. The mixture was transferred into a polytetrafluorethylene-coated stainless-steel autoclave and heated at 180 °C for 20 hours. The sample cooled down freely to room temperature. A light-brown powder was separated via filtration and washed several times with deionized water and absolute ethanol (CH_3CH_2OH, VWR Chemicals, purity 100%). The solid was dried at 60 °C overnight. Finally, the intermediate product was calcinated at 500 °C for 4 hours in a muffle oven in air.

B. High-pressure/high-temperature application

High-pressure/high-temperature experiments were performed using a 1000 t Voggenreiter Walker-type multi-anvil press. The prepared polycrystalline spinel powder (see above) was packed in a crucible of hexagonal boron nitride. This crucible was surrounded by a graphite resistance heater, which was incorporated in a chromium oxide (Cr_2O_3)-doped magnesium oxide octahedron, isolated by a zirconium dioxide (ZrO_2) sleeve. Disks of molybdenum were put at both ends of the capsule and served as a conduction medium for the heater. The sample octahedron was put in the center of eight edge-truncated cubes of tungsten carbide, which were separated against each other with gaskets of pyrophyllite. For the experiments, assemblies of either 14/8 or 10/5 (octahedron edge length in mm/truncation-edge length in mm) were chosen. For the treatment under extreme conditions, the target pressure of 12 GPa was reached by setting a constant ramp of 10 t/h at room temperature. After reaching the pressure limit, a temperature of 500 °C was set by heating the sample with 30 °C/min. The sample was kept for 60 minutes before quenching by turning off the electrical power. The device was decompressed with a rate of 1 t/h. The obtained sample material is named "post-spinel" and consists mainly of the γ-Mn_3O_4 phase as verified by XRD analysis (see below). A similar procedure was repeated for another spinel sample, but with applying milder conditions of only 7.2 GPa and 400 °C that were reported to be sufficient for the transformation of the Mn_3O_4 spinel to the marokite high-pressure modification [21]. Since in this work the obtained material still has the α-Mn_3O_4 structure after application of the milder conditions, but with a high amount of lattice defects/strain (see below), this sample was named "def-spinel".

C. Structure

For structural characterization at room temperature, the samples were filled into 0.5-mm-diameter glass capillaries and measured in Debye-Scherrer geometry in a STOE Stadi P diffractometer using Ag radiation ($\lambda = 0.559360$ Å) equipped with two MYTHEN detectors. Rietveld refinement was performed using FULLPROF [24]. Instrumental Caglioti paramaters U, V, and W were determined by Rietveld refinement to an XRD pattern of LaB_6 reference material [25] from the National Institute of Standards and Technology (NIST). For the spinel and def-spinel samples that consist predominantly of α-Mn_3O_4, the $CdMn_2O_4$ structure type [3,7] was utilized with refinable O atomic position. Individual isotropic temperature displacement factors for Mn [constrained to the same value for Mn(1) and Mn(2)] and for O were refined for the α-Mn_3O_4 phase in the spinel sample. The obtained values were used in a fixed manner for the structural model of the α-Mn_3O_4 phase used for the def-spinel sample. For the post-spinel sample consisting predominantly of the γ-Mn_3O_4 phase, the atomic structure according to the $CaMn_2O_4$ structure type [1,16] was utilized with fixed crystallographic site occupation, but refinable Mn and O atomic positions and individual isotropic temperature displacement factors for Mn(1) and Mn(2), but constrained values for O(1), O(2), and O(3). Microstructural effects such as isotropic crystalline size and strain were treated using the Thompson-Cox-Hastings pseudo-Voigt profile function [26] including Finger's [27] treatment of the axial divergence for the α-Mn_3O_4 phase in the spinel and the γ-Mn_3O_4 phase in the post-spinel sample. For the α-Mn_3O_4 phase in the def-spinel sample, anisotropic strain (only the Gaussian component is taken into account) was considered by an orthorhombic strain model that takes fluctuations along the unit cell directions a, b, and c [24] into account by refinable parameters. The degree of anisotropy is given in brackets after the value of strain in Table I.

In situ low-temperature XRD experiments were performed for the post-spinel sample on a STOE StadiP diffractometer, equipped with an Ag anode and two MYTHEN detectors in Debye-Scherrer geometry using monochromatic radiation ($\lambda = 0.5594$ Å). The sample was hand ground in an agate mortar and placed in an 0.5 mm glass capillary. An Oxford Cryostream Plus (Liquid Nitrogen) was used to cool the sample to 150 K with a cooling rate of 10 K/min. During an isothermal XRD measurement of 50 min, the temperature was held constant. Diffraction patterns were measured at 150, 175, 200, 225, 250, and 275 K. All standard deviations of the refined Rietveld parameters were multiplied by a factor as outlined by Bérar and Lelann [28,29]. The so-obtained correlated residuals are given in brackets (for numerical values), and are plotted as vertical error bars in the graphs.

Mn K-edge XAS measurements were collected in fluorescence mode at the CLÆSS beamline [30] (ALBA CELLS synchrotron, Barcelona, Spain) using a multichannel fluorescence detector placed at 90° with respect to the incoming beam. The synchrotron radiation of a wiggler source was monochromatized by means of a Si(111) double-crystal monochromator. The calibration of the monochromator was performed by measuring the spectrum of a Mn metal foil in transmission mode. The Mn K-edge spectra were measured from 6435 to 7774 eV for the spinel sample at 300 K and for the postspinel sample with mainly γ-Mn_3O_4 phase at 80 and 300 K with the help of a standard liquid nitrogen cryostat (LN2-cryo). For all measurements the sample was within vacuum (10^{-2} bar). The raw data spectra were normalized and background corrected with help of the ATHENA software [31]. The Mn K-edge was found to be located at 6546.4 eV

TABLE I. Results of Rietveld refinement to XRD patterns of the spinel, def-spinel, and post-spinel samples.

Spinel sample					
	α-Mn_3O_4 ($I4_1/amd$)				
	$a = 5.7690(2)$ Å		Avg. size[a] = 159(1) nm		
	$c = 9.4608(5)$ Å		No strain effect indicated		
Atom	x	y	z	occ.[b]	B_{iso} (Å^2)
$Mn(1)/Mn^{2+}$	0	3/4	1/8	1/8	0.55(6)
$Mn(2)/Mn^{3+}$	0	0	1/2	1/4	0.55(6)
O(1)	0	0.469(1)	0.2579(9)	1/2	0.5(2)
					$R_B = 3.69$; $R_F = 3.46$
Def-spinel sample					
	α-Mn_3O_4 ($I4_1/amd$)				
	$a = 5.769(1)$ Å		Avg. size = 47(1) nm		
	$c = 9.459(2)$ Å		Avg. strain = $99(15) \times 10^{-4}$		
Atom	x	y	z	occ.	B_{iso} (Å^2)[c]
$Mn(1)/Mn^{2+}$	0	3/4	1/8	1/8	0.55
$Mn(2)//Mn^{3+}$	0	0	1/2	1/4	0.55
O(1)	0	0.471(2)	0.2587(9)	1/2	0.5
					$R_B = 2.82$; $R_F = 1.44$
Post-spinel sample					
	γ-Mn_3O_4 ($Pbcm$)				
	$a = 3.0251(3)$ Å		No size effect indicated		
	$b = 9.819(1)$ Å		Avg. strain = $60(1) \times 10^{-4}$		
	$c = 9.580(1)$ Å		7.2(5) wt.% α-Mn_2O_3 ($Ia\bar{3}$) additional phase		
Atom	x	y	z	occ.	B_{iso}(Å^2)
$Mn(1)/Mn^{2+}$	0.680(3)	0.1474(6)	1/4	0.5	0.6(1)
$Mn(2)/Mn^{3+}$	0.207(2)	0.3850(5)	0.0700(4)	1.0	0.18(8)
O(1)	0.622(7)	1/4	0	0.5	0.01(20)
O(2)	0.184(8)	0.207(3)	1/4	0.5	0.01(20)
O(3)	0.199(6)	0.472(2)	0.112(1)	1.0	0.01(20)
					Quality of fit of main phase: R_B =4.65; $R_F = 3.81$

[a]As defined in [24].
[b]Specific crystallographic site multiplicity divided by general site multiplicity of corresponding space group.
[c]Values taken from refinement of α-Mn_3O_4 phase of spinel sample.

and for the normalization and the background removal of the spectra, a pre-edge range from −112.128 to −30 eV and a normalization range from 50 to 350 eV were used.

D. Magnetic characterization

Zero-field-cooled (ZFC) and field-cooled (FC) magnetic moment vs temperature scans were measured from 2 to 390 K in sweep mode at a rate of 2 K/min with temperature increment of 1 K at a magnetic field of 0.5 kOe for the spinel and def-spinel sample, and additionally at 0.1, 2.5, and 10 kOe for the post-spinel sample. Full loop magnetic moment vs field scans with maximum field of 70 kOe have been measured in field-cooled mode (FC) at selected temperatures from 2 to 300 K, starting with the lowest temperature. Due to flux line pinning at low fields (less than 10 kOe), the magnetic field at the sample place can deviate up to 10 Oe from the requested field for the 90 kOe superconducting magnet. Small observed hysteresis that are in this field range, up to approximately 10 Oe, cannot be ascribed to the sample, but need to be considered as artifacts [32]. For the spinel sample, consisting of the α-Mn_3O_4 phase, time-dependent magnetization measurements were performed. The sample was cooled from 100 K in zero field to 10, 20, and 55 K, respectively, and the evolution of the magnetic moment has been tracked for about 20 minutes after a field of 1000 Oe has been set with maximum rate of 220 Oe/second. $\Delta M/M_0$ is plotted over time, where M_0 is the temperature corresponding to the magnetic moment after 20 minutes and ΔM is the time-dependent difference to M_0. The ac susceptibility was measured from 250 to 10 K in zero dc magnetic field with an excitation field of 5 Oe for the frequencies 0.1, 1, and 10 kHz (only 1 and 10 kHz for the post-spinel and the def-spinel samples) and an averaging time of 10 seconds per point.

Isobaric heat capacity C_p was measured for the spinel sample from 300 to 5 K with a temperature increment of 5 K, and additionally from 60 to 30 K with a smaller temperature increment of 2 K in zero field and at 30 kOe. For the post-spinel sample, C_p was measured for 40 log-distributed temperatures from 300 to 2 K, and additionally with a 1 K temperature increment from 55 to 48 K. The heat capacity was determined by a total "two-tau" fitting to the heating

TABLE II. Results of Rietveld refinement to XRD patterns obtained by *in situ* low-temperature measurement for the γ-Mn_3O_4 main phase of the post-spinel sample.

	275 K	250 K	225 K	200 K	175 K	150 K	
				Unit cell			$\Delta p/p \times 10^3$
a (Å)	3.0241(4)	3.0231(2)	3.0234(4)	3.0222(4)	3.0217(4)	3.0200(4)	−0.74
b (Å)	9.816(1)	9.816(1)	9.813(1)	9.808(1)	9.808(1)	9.804(1)	−0.84
c (Å)	9.575(1)	9.577(1)	9.576(1)	9.576(1)	9.577(1)	9.574(1)	−0.01
V (Å^3)	284.22(5)	284.19(5)	284.11(5)	283.85(5)	283.84(5)	283.47(5)	−1.59
				Atomic structure			
Mn^{3+}: x	0.183(4)	0.180(3)	0.181(4)	0.185(4)	0.182(4)	0.185(3)	
Mn^{3+}: y	0.3981(7)	0.3978(7)	0.3978(7)	0.3976(7)	0.3972(7)	0.3976(6)	
Mn^{3+}: z	0.044(2)	0.043(2)	0.044(2)	0.045(3)	0.043(2)	0.047(2)	
Mn^{2+}: x	0.6802(5)	0.6804(5)	0.6799(5)	0.6805(5)	0.6806(5)	0.6804(4)	
Mn^{2+}: y	0.1368(6)	0.1367(6)	0.1367(6)	0.1366(6)	0.1363(6)	0.1359(6)	
O(1): x	0.63(1)	0.63(1)	0.62(1)	0.62(1)	0.63(1)	0.631(9)	
O(2): x	0.19(1)	0.19(1)	0.18(1)	0.21(1)	0.22(1)	0.21(1)	
O(2): y	0.200(3)	0.201(3)	0.201(3)	0.199(3)	0.197(3)	0.2006(3)	
O(3): x	0.210(3)	0.216(8)	0.221(9)	0.210(9)	0.214(9)	0.213(8)	
O(3): y	0.473(2)	0.474(2)	0.473(2)	0.470(2)	0.471(2)	0.470(2)	
O(3): z	0.112(2)	0.111(2)	0.112(2)	0.112(2)	0.111(2)	0.111(2)	
				Phase fractions			
γ-Mn_3O_4 (wt.%)	92(2)	91(2)	92(2)	82(2)	86(2)	88(2)	
α-Mn_2O_3(wt.%)	8(1)	8(1)	8(1)	7(1)	7(1)	8(1)	
Ice (wt.%)				11(1)	7(1)	4(1)	
				Quality of fit γ-Mn_3O_4 main phase			
R_B/R_F	4.41/2.49	4.31/2.26	4.58/2.41	2.89/2.15	3.83/2.65	4.12/2.75	

and cooling relaxation curves. Heating was induced by a constant power application that causes a 2% temperature rise. Prior to the sample measurement, addenda measurements were performed. For that purpose only, the sample platform together with some small amount of Apiezon N grease on the platform for improvement of the heat transfer between platform and sample were measured. For the physical property measurements, 10.0(1), 5.1(1), and 9.5(1) mg of the spinel, post-spinel, and def-spinel polycrystalline samples, respectively, were used.

III. RESULTS AND DISCUSSION

A. Structure

The XRD patterns measured at room temperature for the spinel, the post-spinel, and the def-spinel samples are presented in Fig. 1, together with the simulated patterns according to the structural model as obtained by Rietveld refinement. Table I lists the refined structural parameters. The reflections of the XRD pattern obtained for the as-synthesized spinel sample can be ascribed to a tetragonal α-Mn_3O_4 phase (hausmannite) with space group $I4_1/amd$, as shown in Fig. 1(a). As can be inferred from Fig. 1(c), the reflections of the XRD pattern of the post-spinel sample (Mn_3O_4 sample after application of 12 GPa and 500 °C) can be indexed according to an orthorhombic γ-Mn_3O_4 main phase with marokite-type structure (space group $Pbcm$) with a phase fraction of 93(2) wt.% and to an additional minor α-Mn_2O_3 phase [33] (space group no. 206: $Ia\bar{3}$) with a phase fraction of 7.2(5) wt.%. The isotropic temperature displacements factors B_{iso} refined for O of the γ-Mn_3O_4 phase are unreasonably small and should not be considered to represent reliable physical quantities in this case. Furthermore, an apparent strain of $\epsilon = 60(1) \times 10^{-4}$ has been obtained by the Rietveld refinement for this phase. The reflections of the def-spinel sample (Mn_3O_4 sample after application of moderate pressure and temperature, i.e., 7.2 GPa and 400 °C) can be indexed according to a single phase with a tetragonal α-Mn_3O_4 and not to a γ-Mn_3O_4 structure [Fig. 1(b)]. A high value of apparent strain, $\epsilon = 99(15) \times 10^{-4}$ (number in brackets quantifies the orthorhombic anisotropy of strain), and reduced crystallite size of 47(1) nm in this sample cause significantly broadened reflections compared to those of the spinel sample. Since the strain is supposed to be related to a high amount of crystallographic defects introduced by the specific high-pressure/high-temperature application without a transformation to the high-pressure modification (or, alternatively, first a transformation into the high-pressure structure that cannot be metastabilized by quenching and then transforms back), this sample is named def-spinel.

The XRD patterns for the post-spinel sample measured *in situ* at 275, 250, 225, 200, 175, and 150 K are presented in Fig. 2, together with the simulated patterns according to the structural model as obtained by Rietveld refinement. The refined structural parameters are summarized in Table II. Beside the γ-Mn_3O_4 ($Pbcm$) main phase, 7 to 8 wt.% of an α-Mn_2O_3 ($Ia\bar{3}$) additional phase is present at all temperatures, and at 150, 175, and 200 K, additional reflections appear that can be ascribed to a water ice phase (space group no. 186: $P6_3mc$). The lattice parameters a, b, c and the unit-cell volume V of the γ-Mn_3O_4 main phase exhibit a relative change $\Delta p/p$ of -0.74×10^{-3}, -0.84×10^{-3}, -0.01×10^{-3}, and -1.59×10^{-3}, respectively, comparing the values obtained

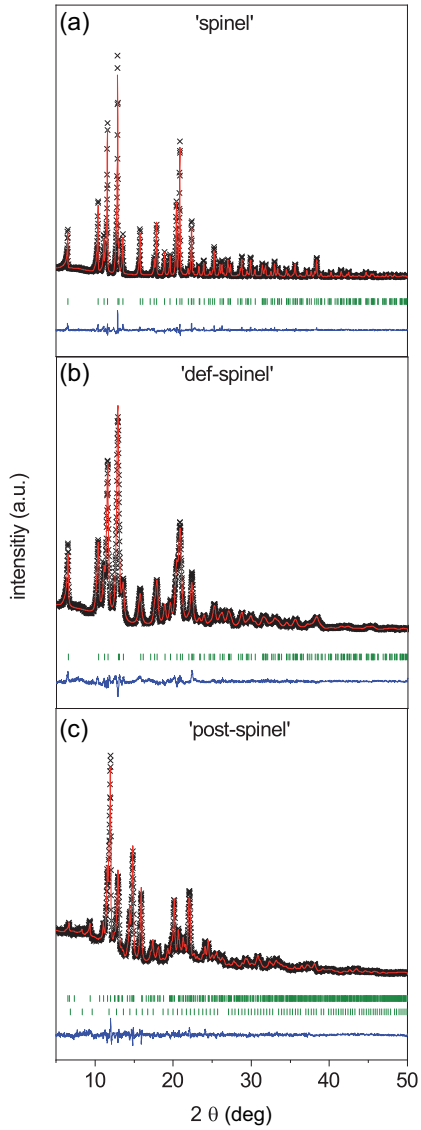

FIG. 1. X-ray diffraction patterns with observed intensities (black crosses), simulated intensities (red line), difference between observed and simulated intensities (blue line), and positions of Bragg reflections (green ticks) for samples (a) spinel with Bragg reflections of α-Mn_3O_4 ($I4_1/amd$), (b) def-spinel with Bragg reflections of α-Mn_3O_4 ($I4_1/amd$), and (c) post-spinel with first row Bragg reflections of γ-Mn_3O_4 (*Pbcm*) and second row Bragg reflections of α-Mn_2O_3 ($Ia\bar{3}$).

at 275 K with those obtained at 150 K. A structural phase transition of γ-Mn_3O_4 at about 210 K is neither indicated by the temperature dependent evolution of these parameters obtained by *in situ* low temperature XRD [see Fig. 3(a)] nor by the Mn K-edge XAS spectra measured at 80 and 300 K [see Fig. 3(b)] that are strongly overlapping. The very small differences in the extended x-ray absorption fine structure (EXAFS) signal that locates in the postedge energy region can at least partially be ascribed to the conventional thermal expansion of the lattice parameters. But if large atomic displacements of the Mn^{2+} species of 0.25 Å along the *a*-direction would have occurred during cooling below 210 K, as claimed in Ref. [22], much stronger changes of the EXAFS signal should be visible instead. The EXAFS curve of isoelectric α-Mn_3O_4, with a different Mn-O coordination, is very different from that of the γ-Mn_3O_4 phase, for instance [Fig. 3(b)]. Hirai *et al.* [22] reported a clear discontinuity around 210 K of the lattice constants *a* and *b* with a unit-cell volume drop of 0.5(1)% based on powder neutron diffraction data and proposed a coupled first-order structural phase transition to occur at this temperature. Moreover, they claimed that the structural phase transition would be connected with giant atomic displacements along the *a* direction of 0.25 Å by the Mn^{2+} ions (4*d* Wyckoff site) and of 0.16 Å by one crystallographic oxygen species O(3) (8*e* Wyckoff site) based on powder neutron diffraction data. According to the results of *in situ* low-temperature XRD of this work, the Mn^{2+} ions (4*d* Wyckoff site) exhibit a maximum atomic displacement of only 0.0174 Å and that of the oxygen species O(3) (8*e* Wyckoff site) of 0.0395 Å, both along the *a* direction. With respect to the question of whether the magnetic phase transition at 210 K is coupled to a structural phase transition, the XRD method applied here offers the advantage to be exclusively sensitive to the atomic structure. Compared to the PND method, there is no need for a discrimination of a structural phase transition from a magnetic phase transition. Especially in the case in which the PND data are of poor quality due to the small sample amounts typically available for metastable high-pressure modifications, such a discrimination might not be possible unambiguously when whole pattern fitting methods such as Rietveld refinement are applied. Giant atomic displacements that were claimed to occur during the coupled magnetic and structural transition in γ-Mn_3O_4 at $T_N' = 210$ K based on the powder neutron diffraction data [22] should therefore be supported by other complementary analytical methods such as XRD and should not rely on PND only. The Mn^{2+} (4*d* Wyckoff site) *x* coordinate determined for γ-Mn_3O_4 (*Pbcm*) at 290 K is listed as 0.876 in Table 1 in Ref. [22] and, under collection code 188903 in the Inorganic Crystal Structure Database (ICSD) [34], as 0.876 (Published Crystal Structure Data) and $0.624 = 1.5 - 0.876$ (Standardized Crystal Structure Data). Table III lists published Mn^{2+} (4*d* Wyckoff site) atomic coordinates obtained for γ-Mn_3O_4 by different diffraction techniques and at different pressures, but all at about room temperature. All of the reported Mn^{2+} (4*d* Wyckoff site) *x* coordinates, which are given in standardized form here, are equal or larger than 0.68, except for that obtained by powder neutron diffraction at 290 K that is given as 0.624 and is the reason for the claimed large atomic shift of 0.25 Å for Mn^{2+} [22]. That means that the unusual large atomic displacement claimed to be present in Ref. [22] actually bases on the determined Mn^{2+} (4*d* Wyckoff site) *x* coordinates at 290 K that deviate considerably from all other published values. It should also be mentioned here that especially the lattice parameter $b = 9.880$ Å, as determined at 290 K in Ref. [22], is considerably larger than $b = 9.819(1)$ Å, as determined in this work at 293 K, and all other published *b* lattice parameters obtained around room temperature, as summarized in Table III, that are even smaller than 9.8 Å.

With respect to this point of controversy, several other inconsistencies of the data given in Ref. [22] should be mentioned here. At first, the lattice parameters of γ-Mn_3O_4

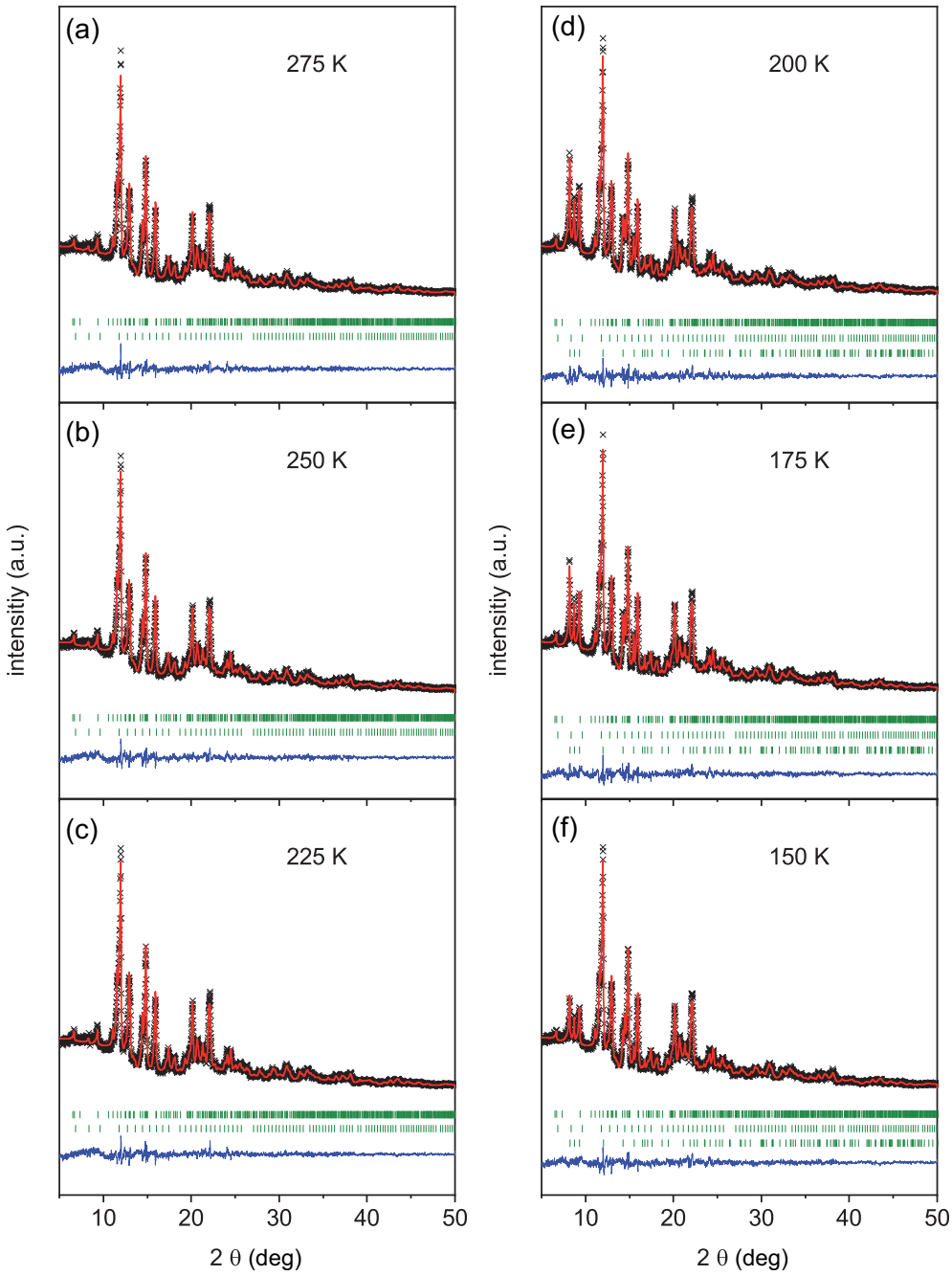

FIG. 2. *In situ* low-temperature XRD of the post-spinel sample with γ-Mn_3O_4 as the main phase at (a) 275, (b) 250, (c) 225, (d) 200, (e) 175, and (f) 150 K. Observed intensities (black crosses), simulated intensities (red line), difference between observed and simulated intensities (blue line), and positions of Bragg reflections (green ticks) with first row Bragg reflections of γ-Mn_3O_4 (*Pbcm*), second row Bragg reflections of α-Mn_2O_3 ($Ia\bar{3}$), and third row Bragg reflections of water ice ($P6_3mc$).

(*Pbcm*) determined at 60 K are given as $a = 3.032$ Å, $b = 9.842$ Å, and $c = 9.568$ Å ($V = a \cdot b \cdot c = 285.52$ Å^3), but the volume of the orthorhombic unit cell is listed in the same table as $V = 284.4$ Å^3. In analogy, the lattice parameters determined at 290 K are given as $a = 3.020$ Å, $b = 9.880$ Å, and $c = 9.583$ Å ($V = a \cdot b \cdot c = 285.93$ Å^3), but the volume is listed as $V = 287.0$ Å^3 (see Table 1 in Ref. [22]). Furthermore, the Mn^{2+} (4*d* Wyckoff site) *x* coordinate determined for γ-Mn_3O_4 (*Pbcm*) at 60 K is listed as 0.760(8) (see Table 1 in Ref. [22]), but as 0.685 for the standardized crystal structure data and $0.815 = 1.5 - 0.685$ for the published crystal structure data in the ICSD. That means that the value given in the ICSD that refers to the same publication [22] is not consistent. The claimed giant atomic displacements of Mn^{2+} and O(3) along the *a* direction [22] are in contradiction to what has been found by *in situ* low-temperature XRD and Mn K-edge XAS in this work and there exist several inconsistencies of published structural data in Table 1 of Ref. [22] and the ICSD (collection code 188902 and 188903) that also refers to Ref. [22]. Therefore, a clarification of the inconsistencies of

TABLE III. Comparison of the lattice parameters and of the Mn^{2+} atomic coordinates of the γ-Mn_3O_4 phase.

a (Å)	b (Å)	c (Å)	x	y	z	Method	Conditions	Collection code[a]	References
3.020(2)	9.880(4)	9.583(3)	*0.6240*	0.1370	0.25	PND[b]	290 K, atm[c]	188903	[22]
3.032(1)	9.842(6)	9.568(4)	0.6850	0.1370	0.25	PND	60 K, atm	188902	[22]
3.026(1)	9.769(2)	9.568(1)	0.6832	0.1453	0.25	SCXRD[d]	rt[e], atm	30005	[35]
3.0240(1)	9.7996(3)	9.5564(3)	0.6845	0.1461	0.25	PXRD[f]	rt, atm	40110	[14]
2.8960(23)	9.5081(56)	9.2587(84)	0.708	0.129	0.25	PXRD	300 K, 21.1 GPa	97867	[16]
2.9968(2)	9.7262(4)	9.514(4)	0.6922	0.1444	0.25	SCSRD[g]	293 K, atm	113668	[1]
2.9279(2)	9.5531(6)	9.373(4)	0.7042	0.1419	0.25	SCSRD	293 K, 15.5 GPa	113672	[1]
2.8838(2)	9.4178(9)	9.283(4)	0.7101	0.1408	0.25	SCSRD	293 K, 26 GPa	113670	[1]
2.8148(4)	9.2161(12)	9.134(7)	0.7165	0.1397	0.25	SCSRD	293 K, 44 GPa	113671	[1]
2.7744(3)	9.0805(12)	9.069(6)	0.7201	0.13945	0.25	SCSRD	293 K, 54.6 GPa	113669	[1]
2.7883(4)	8.998(3)	9.048(6)	0.7226	0.1394	0.25	SCSRD	293 K, 60 GPa	113673	[1]
3.0251(3)	9.819(1)	9.580(1)	0.680	0.1473	0.25	PXRD	293 K, atm		This work
3.0200(4)	9.804(1)	9.574(1)	0.6804(4)	0.1359(6)	0.25	PXRD	150 K, atm		This work

[a]Inorganic Crystal Structure Database (ICSD) [34].
[b]Powder neutron diffraction.
[c]Atmospheric.
[d]Single-crystal x-ray diffraction.
[e]Room temperature.
[f]Powder x-ray diffraction.
[g]Single-crystal synchrotron radiation diffraction.

the published crystal structural data and a reexamination of whether giant atomic displacements of Mn^{2+} and O(3) along the a direction are results of a structural phase transition that is coupled to the magnetic one, as claimed in Ref. [22], are recommended by the authors of this work.

B. Magnetic characterization

1. *Spinel sample* (α-Mn_3O_4)

The dc susceptibility vs temperature curves measured for the spinel sample that consists exclusively of the α-Mn_3O_4 phase reproduce well what has been reported in the literature [7]. The ZFC and FC curves coincide at high temperature and start to bifurcate at $T_{max}^{ZFC} = 40.2(5)$ K, where the ZFC curve exhibits a local maximum [Fig. 4(a)]. This is a characteristic feature of the ZFC/FC branches for a transition from a paramagnetic to a ferri-/ferromagnetic phase where domain-wall movement represents an irreversible process that causes the ZFC/FC bifurcation. T_{max}^{ZFC} is slightly below the Curie temperature $T_C = 42.5$ K, where occurrence of ferrimagnetic ordering has been observed [7]. The inverse susceptibility vs temperature is still slightly bent at the maximal temperature of the experiment of 390 K due to magnetic short-range preordering. From a Curie-Weiss fit from 370 to 390 K, an effective paramagnetic moment of $\mu_{eff} = 4.94(7)\ \mu_B$ per Mn ion and a Weiss constant of $-381(11)$ K have been determined. The values are slightly smaller than those published in Ref. [7] that have been obtained for temperatures above 400 K (see also Table IV). The magnetic moment vs field scans [Fig. 5(a)] at 2, 20, and 40 K confirm the ferrimagnetic nature below the Curie temperature with the coercivity field and the maximum magnetic moment (value at 70 kOe) decreasing with increasing temperature. The zero-field extrapolated magnetic moment at 20 K is $M_S = 1.51(5)\ \mu_B$ per f.u. α-Mn_3O_4 shows the isothermal evolution of magnetization in dependence of time, $\Delta M/M_0$, below T_C as determined by cooling down the sample in ZFC mode before the dc field is applied [Fig. 5(d)]. A double-logarithmic plot of $\Delta M/M_0$ vs time [inset in Fig. 5(d)] shows a linear progression to good approximation within the duration of the experiment of 20 minutes. The evolution can be fitted by a power law of time according to $\Delta M/M_0 = M_A \times t^{\tau}$, where t is the time, M_A is the prefactor or starting value, and τ is the exponent of time evolution. The obtained parameters for the isothermal time-dependent magnetization at 10 and 20 K are presented in Table IV. The ac susceptibility vs temperature curves in Fig. 6(a) show sharp maxima at $\chi'_{max} = 41.0(5)$ K and $\chi''_{max} = 41.0(5)$ K, independently of the excitation frequency. This is a characteristic feature of a transition from paramagnetic to ferri-/ferromagnetic where not only the susceptibility χ' (dispersion) diverges at the magnetic phase transition, but also energy dissipation (absorption) occurs, parametrized by χ'', due to the onset of irreversible processes related to changes of net magnetization (domain-wall movements).

2. *Post-spinel sample (mainly* γ-Mn_3O_4*)*

For the post-spinel sample that mainly consists of the γ-Mn_3O_4 phase, the dc susceptibility vs temperature plots show a cusp at $T_{max}^{ZFC} = 58.5(5)$ K and a very weak, diffuse "hump" at around $T_{max}^{ZFC} = 210(10)$ K, that is most clearly visible for low fields [Fig. 4(b)]. A bifurcation of the ZFC/FC branches is visible below $\sim$150 K and becomes less pronounced the higher the applied dc magnetic field is. For 10 kOe, the ZFC/FC bifurcation is only very weak since the high applied field mainly overcomes the coercivity field of the ferri-/ferromagnet. A Curie-Weiss fit to the inverse susceptibility from 370 to 390 K [see Fig. 4(d)] returns a paramagnetic moment of $\mu_{eff} = 5.1(1)\ \mu_B$ per Mn ion and a Weiss constant of $-360(20)$ K. The slightly different values as compared to those reported by Ovsyannikov *et al.* [1] (see also Table IV)

TABLE IV. Parameters obtained from dc magnetometry, ac susceptibility, heat capacity, and neutron powder diffraction for the spinel sample (α-Mn_3O_4), post-spinel sample (mainly γ-Mn_3O_4), and def-spinel sample (α-Mn_3O_4 with a high degree of lattice defects).

Sample (main) phase	Spinel α-Mn_3O_4	Post-spinel γ-Mn_3O_4	Def-spinel α-Mn_3O_4	Ovsyannikov *et al.* [1] γ-Mn_3O_4	Hirai *et al.* [22] γ-Mn_3O_4
			DC magnetometry		
μ_{eff} per f.u. (μ_B)[a]	4.94(7)	5.1(1)	4.92(7)	5.80[b]	n.d.[c]
Weiss constant θ (K)[a]	−381(11)	−360(20)	−433(12)	−650[b]	
$T_{\text{max}}^{\text{ZFC}}$ (K)[d]	40.2(5)	58.5(5)/210(10)	42.0(5)	55	40-45
ZFC/FC bifurcation (K)	41.0(5)	n.a.[e]	100(10)	n.a.	100(10)
M_S per f.u. at 20 K (μ_B)[f]	1.51(5)	∼0	1.11(5)	∼0	∼1
			Isothermal time-dependent evolution of magnetization		
M_A (s^{-1}) for 10 K[g]	0.6333(1)				
τ for 10 K	0.06467(3)				
M_A (s^{-1}) for 20 K	0.8368(2)				
τ for 20 K	0.02540(4)				
			AC susceptometry		
χ'_{max} (K)[h]	41.0(5)	60(5)	42.0(5)		
χ''_{max} (K)[c]	41.0(5)	n.a.	42.5(5)		
			Heat capacity		
C_p^{max} at 0 T (K)[i]		55(1)/210(10)	44(1)		55/210
C_p^{max} at 3 T (K)			47(1)		
			Diffraction		
PND[j] (K)					(55)/210

[a]Curie-Weiss fit from 370 to 390 K.
[b]Curie-Weiss fit from 300 to 400 K.
[c]Not determined for high-temperature region.
[d]Measured at 0.5 kOe.
[e]Not applicable.
[f]Zero-field extrapolated magnetic moment.
[g]According to the power law $\Delta M/M_0 = M_A \cdot t^{\tau}$.
[h]ac susceptibility measured at 10 kHz.
[i]Local maxima.
[j]Powder neutron diffraction.

are explained by the fact that their Curie-Weiss fit has been done for another range of temperature from 300 to 400 K and that the inverse susceptibility does not exhibit a pure linear behavior below ∼400 K. The inverse susceptibility of γ-Mn_3O_4 begins to deviate from a linear progression and exhibits a slight upturn slightly above 210 K, where a very weak, diffuse hump is also visible in the susceptibility. The XRD analysis for the post-spinel sample revealed the presence of 7.2(5) wt.% α-Mn_2O_3 ($Ia\bar{3}$) additional phase. α-Mn_2O_3 is reported to order antiferromagnetically between 80 and 90 K [36–39] and, indeed, the ZFC/FC susceptibility curves [Fig. 4(b)] for all fields exhibit a slight superimposed reduction below this temperature.

The measured magnetization exhibits a linear dependence on the magnetic field to good approximation [Fig. 5(b)] for all measured temperatures from 2 to 300 K. This is a very important result confirming that γ-Mn_3O_4 is in an antiferromagnetic, respectively, paramagnetic state over the complete investigated temperature region, in contrast to α-Mn_3O_4 (main phase in the spinel and def-spinel sample) that orders ferrimagnetically at low temperature. In detail, for temperatures below approximately 150 K, where the ZFC/FC susceptibility branches start to bifurcate in the given post-spinel sample, a small hysteresis as characteristic for ferri-/ferromagnetic phases can be observed that are not present for higher temperatures [left inset in Fig. 5(b)]. Either they are related to small amounts of a ferri-/ferromagnetic impurity phase, as also speculated in Ref. [1] where a weak hysteretic signature was observed at 1.8 K, or, alternatively, they are related to some sort of crystallographic defects that cause part of the Mn magnetic moments to exhibit slow magnetic relaxation. The presence of defects is indicated to some extent by significant lattice strain that was refined by Rietveld refinement to the reflections of the γ-Mn_3O_4 phase (see Table I). At 2 K, the remanent magnetization at zero field is only about $1.28 \cdot 10^{-3}$ μ_B per f.u. (compared to 0.240 μ_B at 70 kOe), i.e., the irreversible contribution that causes the very small hysteretic effect is comparably small. Still it has a strong effect on the ZFC/FC bifurcation of the susceptibility measurement that is standardly measured at very low magnetic field. It is important to realize here that this small ferro/ferrimagnetic contribution as found for the post-spinel sample is three orders of magnitude smaller than those found for the spinel and def-spinel samples. For the latter two samples, the whole α-Mn_3O_4 main phase orders ferrimagnetically, whereas the post-spinel sample (i.e., γ-Mn_3O_4) orders antiferromagnetically, but only exhibits very small amounts of a ferro-/ferrimagnetic impurity phase.

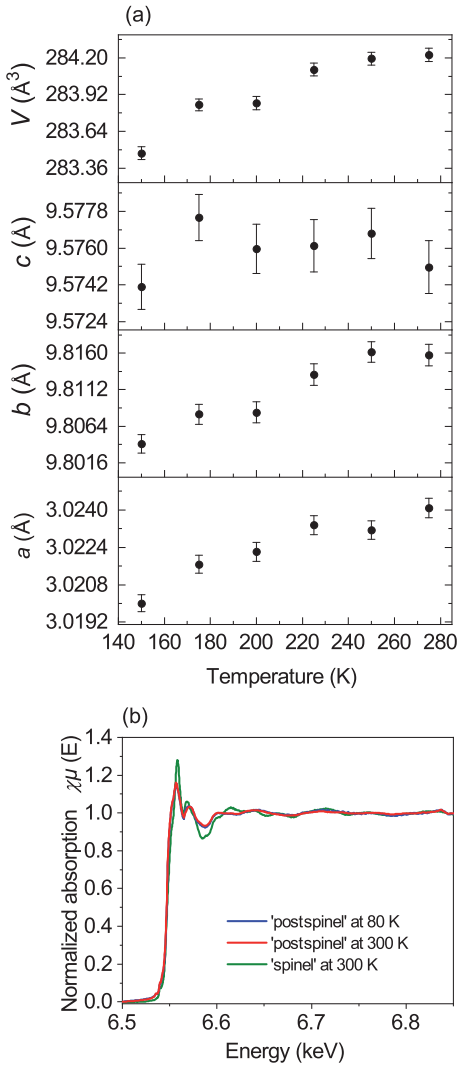

FIG. 3. (a) Lattice parameters a, b, and c and unit cell volume V of γ-Mn_3O_4 main phase in dependence of temperature as obtained by Rietveld refinement of the respective structural models, based on *in situ* low temperature XRD data measured for the postspinel sample. See experimental section for explanation of vertical bars. (b) Sections of synchrotron Mn K-edge XAS spectra measured at 80 and 300 K for the post-spinel sample (γ-Mn_3O_4 main phase) and for the α-Mn_3O_4 spinel sample.

The real part of the ac susceptibility [Fig. 6(b)] shows a cusp at $\chi'_{max} = 60(5)$ K, but the imaginary part χ'' approximately remains constant over the whole temperature range. It should be noted that the maximum ac susceptibility values measured for the post-spinel sample are about two orders of magnitude smaller than the maximum values found for the spinel and def-spinel sample. The large maximum values of the latter two are ascribed to the paramagnetic to ferrimagnetic phase transition that causes the magnetic dispersion χ' to diverge, but also causes χ'' to exhibit a local maximum due to energy dissipating processes that are most pronounced at the temperature of the phase transition (with a coincidence of the onset of χ'' with the maximum of χ'). In contrast to that, for γ-Mn_3O_4 of the post-spinel sample, there are only transitions from paramagnetic to antiferromagnetic ordering involved, that neither show a divergence of χ' nor any energy dissipation as parameterized by χ'' at the phase transition. As a consequence, there is only a cusp in the χ' signal at about 60 K, where all magnetic moments of the Mn ions order antiferromagnetically. The (partial) paramagnetic to antiferromagnetic phase transition also becomes apparent from the λ peak in the heat capacity signal at $C_p^{max} = 55(1)$ K, in agreement with the temperature of transition as obtained from magnetometry. The feature of the broad, diffuse "hump" in the susceptibility data at around 210 K is also reproduced in the heat capacity data by a broad local maximum around this temperature [Fig. 6(d)]. Finally, it should be mentioned that for dc magnetic fields of 0.1 and 0.5 kOe, another small hump in the ZFC branch can be observed at about 34(1) K [marked by stars in Fig. 4(b)] that might point to a further magnetic phase transition that has not been reported in the literature so far for the γ-Mn_3O_4 phase to the best knowledge of the authors.

3. Def-spinel sample (α-Mn_3O_4)

Besides the spinel and the post-spinel samples, the def-spinel sample, consisting of the α-Mn_3O_4 phase with a high amount of lattice defects, has been included in the series of investigation. Figure 4(c) shows the susceptibility that is quite similar to that of what has been measured for the spinel sample. From the Curie-Weiss fit from 370 to 390 K, a paramagnetic moment of $\mu_{eff} = 4.92(7)$ μ_B per Mn ion and a Weiss constant of $-433(12)$ K have been determined. The ZFC branch exhibits a cusp at $T_{max}^{ZFC} = 42.0(5)$ K that is quite close to the ZFC cusp found for the spinel sample consisting of the α-Mn_3O_4 phase (see Table IV). However, the temperature where the ZFC/FC branches start to bifurcate does not coincide with the cusp in the ZFC curve (as approximately for the spinel sample), but is much higher at about 100 K. Like the spinel sample, the def-spinel sample also shows a ferrimagnetic ordering below ~42 K with clear hysteresis and the coercivity fields getting smaller with increasing temperature [Fig. 5(c)]. It should be noted that in contrast to the spinel sample, the magnetization at maximum field is higher for 20 K as compared with the values for 2 and 40 K, i.e., the antiferromagnetic character seems to dominate at lowest temperatures again. The field scan at 20 K exhibits a zero-field extrapolated magnetic moment of $M_S \sim 1$ μ_B per f.u. As shown in the inset of Fig. 5(c), there is still a weak coercivity observable that vanishes for 100 K, in agreement with the bifurcation of the ZFC/FC branch. This irreversible behavior below approximately 100 K that causes the ZFC/FC to slightly bifurcate might either be related to the lattice defects that are present in the α-Mn_3O_4 phase of the def-spinel sample and that might be connected with antisite defects or any other type of modified local structure that results in a slow magnetic relaxation. The presence of small amounts of β-MnO_2 impurity phase with a reported bifurcation below approximately 100 K [40] cannot be ruled out either. However, there are no clear indications for the existence of an impurity phase beside an α-Mn_3O_4 phase from the XRD pattern. The ac susceptibility data for the def-spinel phase are very similar to that measured for the spinel sample with $\chi'_{max} = 42.0(5)$ K and $\chi''_{max} = 42.5(5)$ K independently of the excitation frequency [Fig. 6(c)]. The heat capacity for the def-spinel sample exhibits a local maximum at

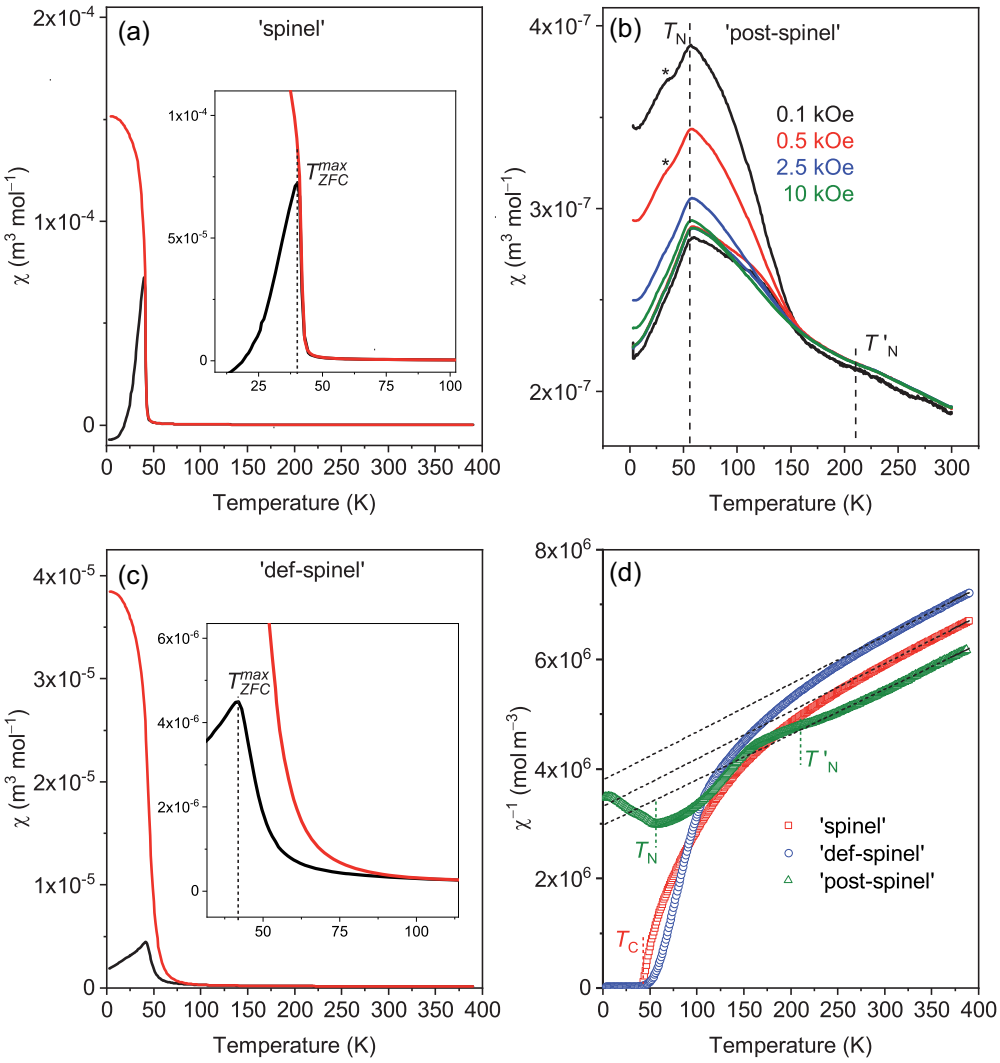

FIG. 4. The dc susceptibility: (a) ZFC (black) and FC (red) susceptibility curves obtained for the spinel sample (α-Mn_3O_4) at 500 Oe. (b) ZFC and FC susceptibility curves for various magnetic fields obtained for the post-spinel sample (mainly γ-Mn_3O_4 phase). (c) ZFC (black) and FC (red) susceptibility curves obtained for the def-spinel sample (α-Mn_3O_4 with high amount of lattice defects) at 500 Oe. (d) Inverse susceptibility curves for all samples derived from ZFC curves measured at 500 Oe together with a Curie-Weiss fit from 370 to 390 K (solid line) and extrapolation (dashed line).

$C_p^{\max} = 44(1)$ K in the zero field that shifts to $C_p^{\max} = 47(1)$ K in a magnetic field of 30 kOe, confirming the ferrimagnetic ordering of the low-temperature phase [Fig. 6(d)]. In summary, the magnetic properties of the def-spinel sample are very similar to those of the spinel sample, both exclusively consisting of the α-Mn_3O_4 phase, with a transition from paramagnetic to ferrimagnetic at about 42 K. The only difference is that the def-spinel sample shows an additional ZFC/FC bifurcation below ∼100 K due to the defects present in α-Mn_3O_4 or due to an additional ferri-/ferromagnetic impurity phase.

4. Discussion of magnetic properties

All results from dc susceptibility and field scans that have been reported by Ref. [22] for what was assumed to be the metastable high-pressure γ-Mn_3O_4 modification actually totally resemble the results obtained for the def-spinel sample (α-Mn_3O_4 with high amount of defects) in this work. The ZFC/FC susceptibilities obtained at 100 Oe, shown in Ref. [22], are quasi-identical with those shown for the def-spinel sample in Fig. 4(c) in this work. Also the results of the field scans (Fig. 5 in Ref. [22]), where a remanent magnetic moment of $M_S \sim 1\ \mu_B$ per f.u. has been reported for 20 K, are in total agreement with what was found for the def-spinel [Fig. 5(c)] in this work. Referring to Ref. [22], it seems that the neutron diffraction experiments as well as the heat capacity measurements were indeed conducted on a γ-Mn_3O_4 phase sample, but that the susceptibility measurements and field scans have accidently been performed on a sample that is very closely related to the def-spinel sample presented in this work. Such a α-Mn_3O_4 phase with high amount of lattice defects might have been obtained unintendedly in Ref. [22] by the attempt to prepare the γ-Mn_3O_4 phase by a high-pressure/high-temperature application. Either the maximum applied pressure might have been insufficient for a successful transformation or, alternatively, the γ-Mn_3O_4 phase might not

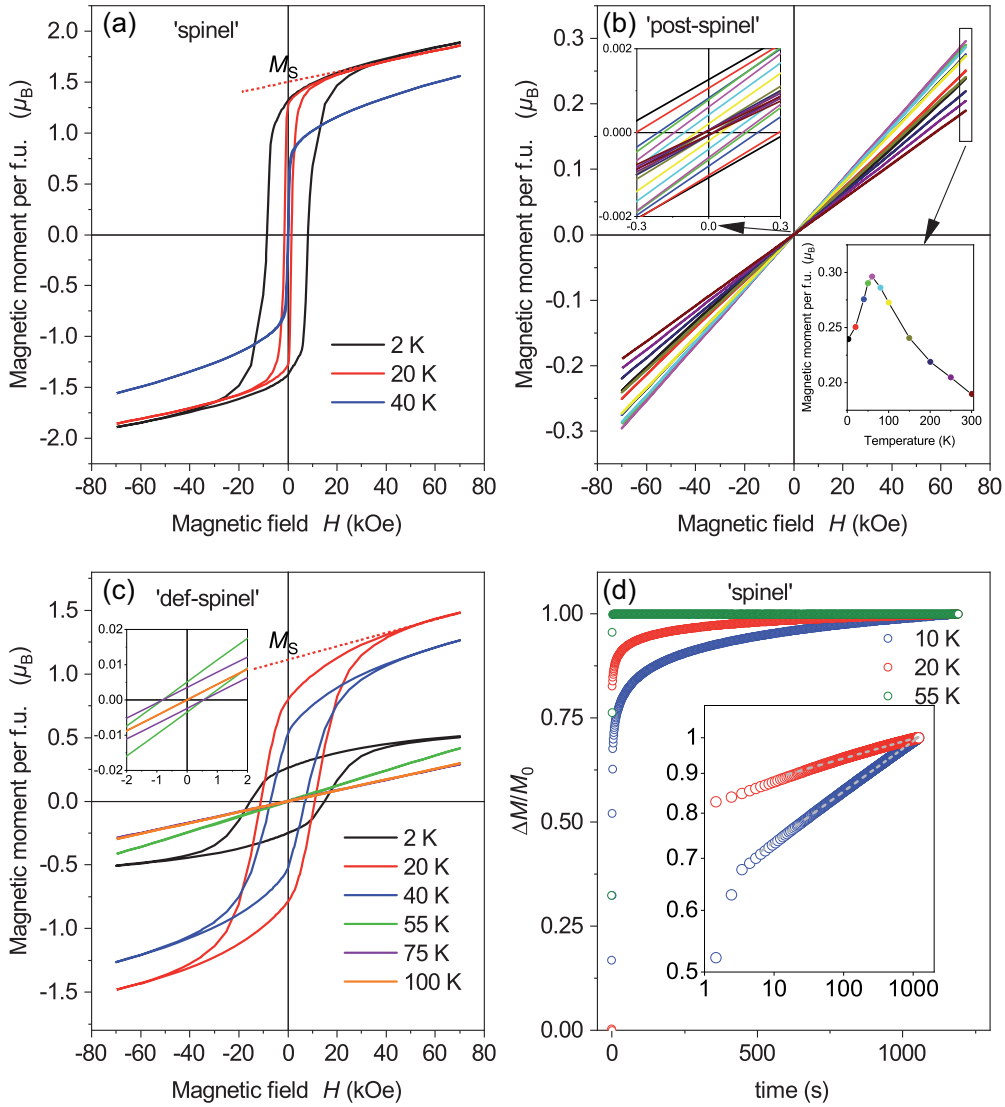

FIG. 5. The dc magnetometry: Field scans for the (a) spinel sample (α-Mn_3O_4) together with zero-field extrapolation of magnetization at 20 K, (b) post-spinel sample (mainly γ-Mn_3O_4 phase) with the evolution of the magnetization at 70 kOe for various temperatures as extracted from field scans (inset at the right bottom), and (c) def-spinel sample (α-Mn_3O_4 with high amount of defects). (d) Isothermal time-dependent change of magnetization for the spinel sample (α-Mn_3O_4 phase) that was zero-field cooled from 100 K to the corresponding temperature before a dc field of 1000 Oe was applied. Double-logarithmic plot of $\Delta M/M_0$ vs time of the isothermal evolution of magnetization at 10 and 20 K together with a time-dependent power-law fit (dashed lines).

have been stabilized in a metastable state due to an inappropriate quenching procedure. On the other hand, the results presented here for γ-Mn_3O_4 (post-spinel sample) are in total agreement with what has been reported for γ-Mn_3O_4 in Ref. [1]. Consequently, the difference of the two characterizations of the nominal γ-Mn_3O_4 phase cannot be explained by the slightly different chemical composition of the investigated γ-Mn_3O_4 compound as suggested in Ref. [1], but needs to be ascribed to the presence of two totally different phases, i.e., γ-Mn_3O_4, on the one hand, and α-Mn_3O_4 with lattice defects, on the other hand.

IV. CONCLUSION

In conclusion, the results from dc and ac magnetometry as well as those from heat capacity measurements found for the metastable high-pressure phase γ-Mn_3O_4 in this work support the existence of a magnetic phase transition from paramagnetic to a partial antiferromagnetic order (only Mn^{3+} ions affected) at 210 K and another magnetic transition at 55 K to an antiferromagnetic order that includes all Mn ions. The existence of these two magnetic phase transitions was initially concluded mainly from powder neutron diffraction and heat capacity measurements [22]. Their existence is also in good agreement with dc magnetometry data presented in another work [1]. However, the dc magnetometry measurement as published in Ref. [22] was unintendedly obtained for an α-Mn_3O_4 phase possessing a high amount of lattice defects that are supposed to have formed during an unsuccessful attempt to metastabilize the high-pressure modification by a quenching process. The dc and ac susceptibility measurements of that α-Mn_3O_4 phase with a high amount of lattice defects are very similar to those of the conventional α-Mn_3O_4

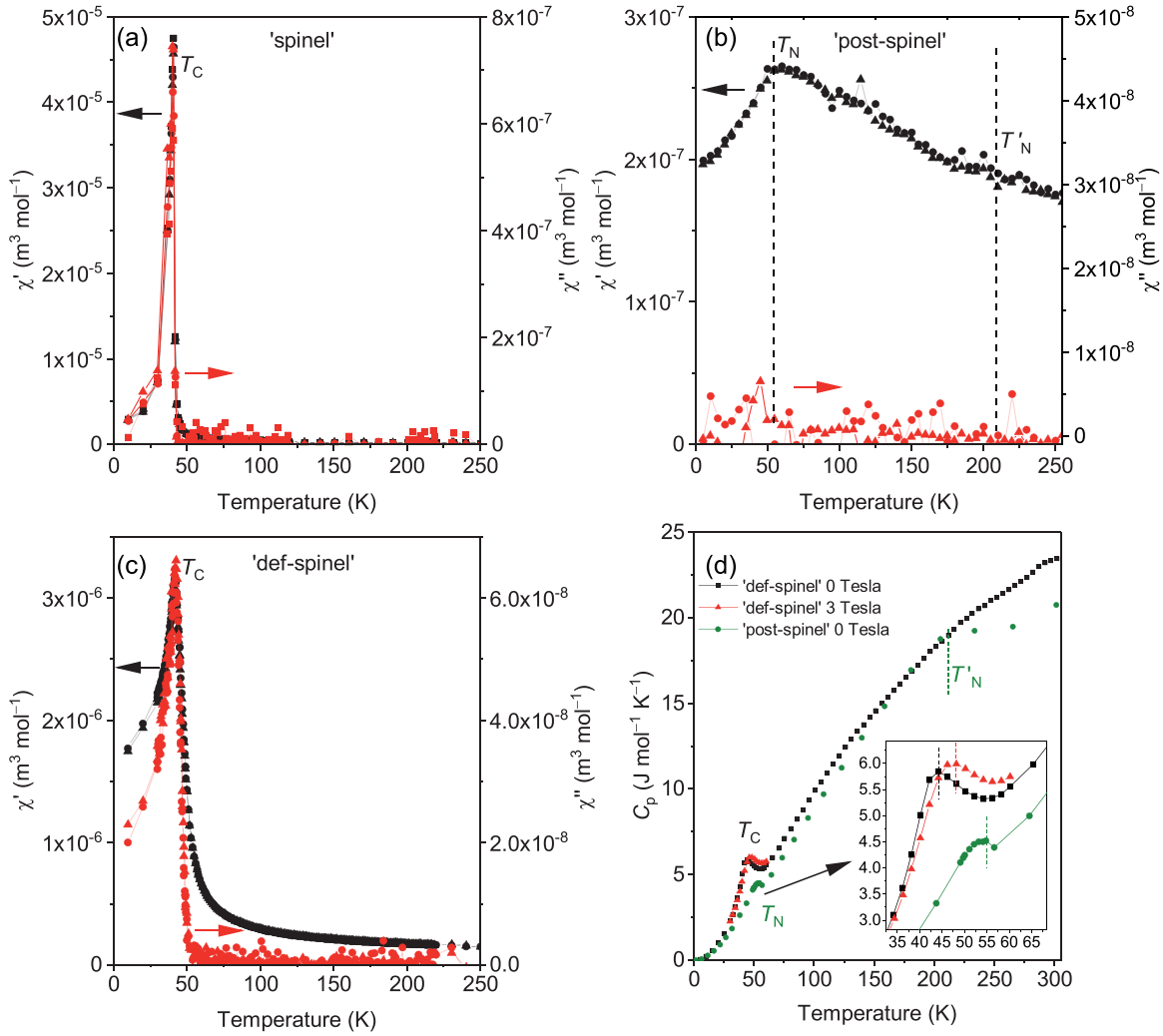

FIG. 6. Real χ' (black) and imaginary χ'' (red) part of the ac susceptibility with 0.1 (square), 1 (circle), and 10 kHz (triangle) excitation frequency for (a) the spinel sample (α-Mn_3O_4), (b) for the post-spinel sample (mainly γ-Mn_3O_4 phase), only measured at 1 and 10 kHz, and (c) for the def-spinel sample (α-Mn_3O_4 phase with high amount of lattice defects), only measured at 1 and 10 kHz. (d) Isobaric heat capacity vs temperature for the def-spinel sample at 0 and 30 kOe (3 T) and for the post-spinel sample at 0 kOe.

phase with a transition from paramagnetic to ferrimagnetic at about 42 K. The difference is a slight bifurcation of the ZFC and FC dc susceptibility curves that is already present below ≈100 K. Most probably, some of the Mn magnetic moments that are located in the direct vicinity of the lattice defects suffer from slow magnetic relaxation and cause the observed irreversibility in the susceptibility curves. Neither the results from *in situ* low temperature XRD nor those from Mn K-edge XAS measured at 80 and 300 K of γ-Mn_3O_4 give any indication for a structural phase transition to be present at about 210 K, where a magnetic phase transition was confirmed by neutron diffraction, susceptibility and heat capacity measurements. Therefore, a coupled structural and magnetic phase transition with giant atomic displacements of the Mn^{2+} ions of about 0.25 Å, as claimed to be found from results of powder neutron diffraction alone in the literature [22], cannot be confirmed by the results obtained for the post-spinel sample consisting mainly of γ-Mn_3O_4 in this work.

ACKNOWLEDGMENTS

The XAS experiments were performed at CLÆSS beamline at ALBA CELLS synchrotron (Barcelona, Spain) with the collaboration of ALBA staff. The authors thank L. Simonelli for her support to perform the low temperature XAS experiments.

[1] S. V. Ovsyannikov, A. A. Aslandukova, A. Aslandukov, S. Chariton, A. A. Tsirlin, I. V. Korobeynikov, N. V. Morozova, T. Fedotenko, S. Khandarkhaeva, and L. Dubrovinsky, Structural stability and properties of marokite-type γ-Mn_3O_4, Inorg. Chem. **60**, 13440 (2021).

[2] H. J. Van Hook and M. L. Keith, The system Fe_3O_4-Mn_3O_4, Am. Mineral. **43**, 69 (1958).

[3] G. Aminoff, XXVIII. About the crystal structure of hausmannite ($MnMn_2O_4$), Z. Kristallogr. **64**, 475 (1926).

[4] K. Satomi, Oxygen positional parameters of tetragonal Mn_3O_4, J. Phys. Soc. Jpn. **16**, 258 (1961).

[5] D. Jarosch, Crystal structure refinement and reflectance measurements of hausmannite, Mn_3O_4, Mineral. Petrol. **37**, 15 (1987).

[6] J. S. Kasper, Magnetic structure of hausmannite, Mn_3O_4, Am. Phys. Soc. **4**, 178 (1959).

[7] B. Boucher, R. Buhl, and M. Perrin, Properties and magnetic structure of Mn_3O_4, J. Phys. Chem. Solids **32**, 2429 (1971).

[8] G. B. Jensen and O. V. Nielsen, The magnetic structure of Mn_3O_4 hausmannite between 4.7 K and Neel point, 41 K, J. Phys. C **7**, 409 (1974).

[9] B. Chardon and F. Vigneron, Mn_3O_4 commensurate and incommensurate magnetic structures, J. Magn. Magn. Mater. **58**, 128 (1986).

[10] M. C. Kemei, J. K. Harada, R. Seshadri, and M. R. Suchomel, Structural change and phase coexistence upon magnetic ordering in the magnetodielectric spinel Mn_3O_4, Phys. Rev. B **90**, 064418 (2014).

[11] T. Suzuki and T. Katsufuji, Magnetodielectric and magnetoelastic properties of spinel Mn_3O_4, J. Phys.: Conf. Ser. **150**, 042195 (2009).

[12] J.-H. Chung, J.-H. Kim, S.-H. Lee, T. J. Sato, T. Suzuki, M. Katsumura, and T. Katsufuji, Magnetic excitations and orbital physics in the ferrimagnetic spinels MnB_2O_4 (B = Mn, V), Phys. Rev. B **77**, 054412 (2008).

[13] A. F. Reid and A. E. Ringwood, Newly observed high pressure transformations in Mn_3O_4, $CaAl_2O_4$, and $ZrSiO_4$, Earth Planet. Sci. Lett. **6**, 205 (1969).

[14] C. R. II Ross, D. C. Rubie, and E. Paris, Rietveld refinement of the high-pressure polymorph of Mn_3O_4, Am. Mineral. **75**, 1249 (1990).

[15] E. Paris, C. R. Ross Il, and H. Olijnyk, Mn_3O_4 at high pressure: A diamond-anvil cell study and a structural modelling, Eur. J. Mineral. **4**, 87 (1992).

[16] Y. Moritomo, Y. Ohishi, A. Kuriki, E. Nishibori, M. Takata, and M. Sakata, High-pressure structural analysis of Mn_3O_4, J. Phys. Soc. Jpn. **72**, 765 (2003).

[17] H. Lv, M. Yao, Q. Li, Z. Li, B. Liu, R. Liu, S. Lu, D. Li, J. Mao, X. Ji, J. Liu, Z. Chen, B. Zou, T. Cui, and B. Liu, Effect of grain size on pressure-induced structural transition in Mn_3O_4, J. Phys. Chem. C **116**, 2165 (2012).

[18] J. Li, B. Liu, J. Dong, C. Li, Q. Dong, T. Lin, R. Liu, P. Wang, P. Shen, Q. Li, and B. Liu, Size and morphology effects on the high pressure behaviors of Mn_3O_4 nanorods, Nanoscale Adv. **2**, 5841 (2020).

[19] G. D. Mukherjee, S. N. Vaidya, and C. Karunakaran, High pressure and high temperature studies on manganese oxides, Phase Trans. **75**, 557 (2002).

[20] X. Liu, S. Xu, K. Kato, and Y. Moritomo, Pressure-induced phase transition in Mn_3O_4 as investigated by Raman spectroscopy, J. Phys. Soc. Jpn. **71**, 2820 (2002).

[21] J. Darul, C. Lathe, and P. Piszora, Mn_3O_4 under high pressure and temperature: Thermal stability, polymorphism, and elastic properties, J. Phys. Chem. C **117**, 23487 (2013).

[22] S. Hirai, A. M. dos Santos, M. C. Shapiro, J. J. Molaison, N. Pradhan, M. Guthrie, C. A. Tulk, I. R. Fisher, and W. L. Mao, Giant atomic displacement at a magnetic phase transition in metastable Mn_3O_4, Phys. Rev. B **87**, 014417 (2013).

[23] D. P. Kozlenko, N. T. Dang, S. E. Kichanov, L. T. P. Thao, A. V. Rutkaukas, E. V. Lukin, B. N. Savenko, N. Tran, D. T. Khan, L. V. Truong-Son, L. H. Khiem, B. W. Lee, T. L. Phan, N. L. Phan, N. Truong-Tho, N. N. Hieu, T. A. Tran, and M. H. Phan, High pressure enhanced magnetic ordering and magnetostructural coupling in the geometrically frustrated spinel Mn_3O_4, Phys. Rev. B **105**, 094430 (2022).

[24] T. Roisnel and J. Rodríquez-Carvajal, WINPLOTR: A windows tool for powder diffraction pattern analysis, Eur. Powder Diffr. **378-381**, 118 (2001).

[25] D. Black, M. Mendenhall, C. Brown, A. Henins, J. Filliben, and J. Cline, Certification of Standard Reference Material 660c for powder diffraction, Powder Diffr. **35**(1), 17 (2020).

[26] P. Thompson, D. E. Cox, and J. B. Hastings, Rietveld refinement of Debye-Scherrer synchrotron x-ray data from Al_2O_3, J. Appl. Crystallogr. **20**, 79 (1987).

[27] L. W. Finger, D. E. Cox, and A. P. Jephcoat, A correction for powder diffraction peak asymmetry due to axial divergence, J. Appl. Cryst. **27**, 892 (1994).

[28] J. F. Bérar and P. Lelann, E.S.D.'s and estimated probable error obtained in Rietveld refinements with local correlations, J. Appl. Cryst. **24**, 1 (1991).

[29] J. K. Stalick, Accuracy in powder diffraction II: A report on the second international conference, J. Res. Natl. Inst. Stand. Technol. **98**, 241 (1993).

[30] L. Simonelli, C. Marini, W. Olszewski, M. Ávila Pérez, N. Ramanan, G. Guilera, V. Cuartero, and K. Klementiev, CLÆSS: The hard X-ray absorption beamline of the ALBA CELLS synchrotron, Cogent Phys. **3**, 1231987 (2016).

[31] B. Ravel and M. Newville, ATHENA, ARTEMIS, HEPHAESTUS: data analysis for X-ray absorption spectroscopy using IFEFFIT, J. Synchrotron Rad. **12**, 537 (2005).

[32] Quantum Design, *Using PPMS Superconducting Magnets at Low Fields: Application Note 1070-207* (Quantum Design San Diego, CA, 2009).

[33] S. Geller, Structure of α-Mn_2O_3, $(Mn_{0.983}Fe_{0.017})_2O_3$ and $(Mn_{0.37}Fe_{0.63})_2O_3$ and relation to magnetic ordering, Acta Cryst. B **27**, 821 (1971).

[34] G. Bergerhoff and I. D. Brown, *Crystallographic Databases* (F.H. Allen et al., Chester, 1987).

[35] L. M. Kuznetsov, A. N. Tsvigunov, and K. P. Brudina, Pressure diagram of manganese(II,III) oxide and crystal structure of the high pressure phase of δ-manganese(II,III) oxide, Geokhimiya **1979**, 254 (1979).

[36] R. G. Meisenheimer and D. L. Cook, Magnetic susceptibility of manganese sesquioxide at temperatures from 4 to 700 K, J. Chem. Phys. **30**, 605 (1959).

[37] R. W. Grant, S. Geller, J. A. Cape, and G. P. Espinosa, Magnetic and crystallographic transitions in the α-Mn_2O_3-Fe_2O_3 system, Phys. Rev. **175**, 686 (1968).

[38] M. Regulski, R. Przeniosło, I. Sosnowska, D. Hohlwein, and R. Schneider, Neutron diffraction study of the magnetic structure of α-Mn_2O_3, J. Alloys Compd. **362**, 236 (2004).

[39] R. R. Chevalier, G. Roult, and E. F. Bertaut, Investigation of the Mössbauer effect in $Mn_{2-x}Fe_xO_3$ and the magnetic transitions in Mn_2O_3 by neutron diffraction, Solid State Commun. **5**, 7 (1967).

[40] T. Barudžija, V. Kusigerski, N. Cvjetićanin, S. Šorgić, M. Perović, and M. Mitrić, Structural and magnetic properties of hydrothermally synthesized β-MnO_2 and α-$KMnO_2$ nanorods, J. Alloys Compd. **665**, 261 (2016).